

Influence of asymmetric long-range interactions on corner states in photonic higher-order topological insulators

José A. Medina-Vázquez *

*Centro de Investigación en Materiales Avanzados S.C., Complejo Industrial Chihuahua,
Miguel de Cervantes 120, C.P. 31136, Chihuahua, México*



(Received 6 January 2023; accepted 3 April 2023; published 12 April 2023)

The introduction of long-range interaction (LRI) in models that describe topological systems has unveiled previously unknown topological phases and states. Recently, in higher-order topological insulators, consideration of LRI via next-nearest-neighbor (NNN) hopping led to the discovery of unconventional confined corner states; however, their study is still limited in photonic prospects. In this paper, we bring the concept of type-III corner states into the photonic regime and reveal that their existence depends on LRI in photonic lattices, mimicking an extended two-dimensional Su-Schrieffer-Heeger (SSH) model with an asymmetric coupling. The extension of the SSH model is performed by considering a variety of NNN hopping in square lattices, and an asymmetry coupling in the intercellular NNN hopping terms of the Hamiltonian describing the system. Subsequently, we identify type-I, type-II, and type-III corner states in the analytical tight-binding model, revealing that the type-II and type-III corner states are split from the edge states. Based on the obtained results, we propose a photonic model that mimics the asymmetric coupling and find the existence of type-II and type-III corner states in the photonic model. The results presented here extend the knowledge we have about topological corner states in photonic systems and highlight the role played by LRIs in the generation of topological confined modes.

DOI: [10.1103/PhysRevA.107.043503](https://doi.org/10.1103/PhysRevA.107.043503)

I. INTRODUCTION

Topological physics has been an exciting research area and has gained remarkable development [1–3]. Several topological phases have been extensively studied in quantum and classical systems such as photonics, phononics, and electric circuits [4–11]. In this regard, topological insulators host topologically protected states with $(D-1)$ dimensionality within the band gap, governed by the celebrated bulk-boundary correspondence [7–11]. Inspired by these discoveries, higher-order topological insulators (HOTIs) emerged as a new class of topological systems with robust confined states, generalizing the bulk-boundary correspondence of topological phases, so that an n th-order topological phase in D dimensions has protected features, at its $(D-n)$ -dimensional boundaries [12–27]. These confined states known as corner states in two-dimensional material, governed by the generalized bulk-boundary-corner correspondence, are promising candidates for topological resonators and lasers [28–31]. In most cases, corner states manifest within a band gap, but they can also appear even if they are spectrally degenerate with the bulk bands [32–34].

In general, the physics of such topological systems can be understood by tight-binding models, which involve only nearest-neighbor (NN) interactions. However, it is not appropriate to consider only NN interactions in the photonic case since long-range interaction (LRI) can significantly alter the band structure [35,36]. Recently, LRIs have been introduced

into systems describing HOTI phases [37–42]. In this sense, there has been significant interest in how LRIs play their role in dictating the behavior of topological phases. For instance, in the presence of weak LRI, type-II corner states have been observed in photonic crystals (PhCs) with kagome lattices [35]. Meanwhile, the addition of LRI by means of additional next-nearest-neighbor (NNN) hopping terms has led to the localization of zero-energy corner states isolated from any bulk or edge band in electronic networks [40]. Therefore, several investigations have pointed out that the addition of higher-order couplings, such as the coupling between NNNs, can preserve the topological protection of the corner states even when the chiral symmetry is broken [43–47]. As an extension of higher-order states and the role played by LRIs, recently, the first identification of type-III corner states in kagome electrical circuits, produced by the splitting of edge states, was achieved [48]. Nevertheless, type-III corner states have not been observed in square lattices or photonic systems. Additionally, the great success of electrical circuit lattices has overshadowed the study of LRI in the HOTI phases of photonic systems.

In this paper, we study the effect of LRIs in an extended two-dimensional Su-Schrieffer-Heeger (SSH) model with a square lattice. We find that introducing asymmetric hopping terms between NNNs can lead to the existence of type-II and type-III corner states in square lattices. We also compared the asymmetric coupling between NNNs with a symmetric coupling, demonstrating that in the latter only the type-I and type-II corner states exist, as other works report [35]. As the coupling strength between the NNNs decreases, we find that also the type-II corner states disappear, merging with

*jose.medina@cimav.edu.mx

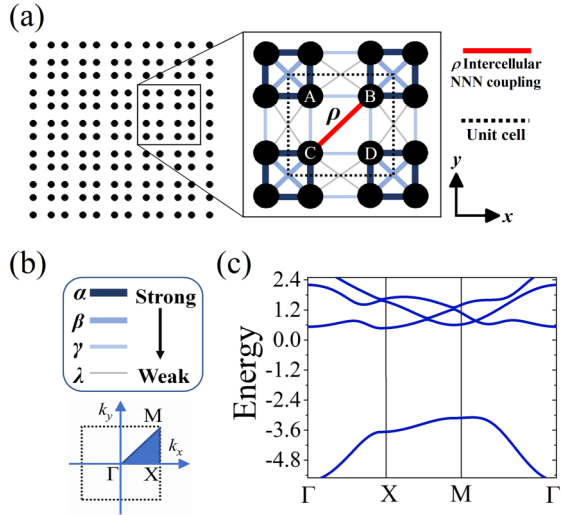


FIG. 1. Schematic representation of the extended 2D SSH model on a square lattice, represented by the Hamiltonian of Eq. (1). On the right is shown an amplification of a unit cell, delimited with a square of dashed lines, and consisting of four sites per unit cell (A–D). The red line stands for asymmetric intercellular coupling. (b) The amplitude of the hopping is represented by lines whose thickness indicates the coupling strength being α the strongest and γ the weakest. (c) Band diagram obtained from the tight-binding model and the extended SSH Hamiltonian with the asymmetric coupling ρ .

the topological edge states, leaving only the type-I corner states. Having confirmed the existence of type-III corner states in the tight-binding model, we propose a simple design that allows finding the corner states in PhCs using first-principles calculations. The photonic structure under study consists of a PhC slab with a square lattice and elliptical air holes. Here, the elliptical geometry facilitates the coupling between the NNNs. We confirm that in the designed PhC slab, the type-III corner states arise as confined states around the topological corner of the proposed photonic systems. In addition, the field distribution coincides with the probability density calculated by means of the tight-binding model. The results we present here broaden the concept of corner states in photonic systems and provide ideas for the generation of confined states in topological systems.

II. EXTENDED SSH MODEL

The extended SSH model with a square lattice considered in this paper is shown in Fig. 1(a). The lattice geometry applies easily to a wide variety of physical systems. This extended model differs from the original SSH model, where only the coupling between NNs is considered. Here, we also consider the couplings between the NNNs, as shown in the amplification of the proposed topological lattice shown in Fig. 1(a). In topological systems, NNN hopping terms can be regarded as LRIs since higher-order terms beyond NNN can only contribute to negligible effects [35,39]. The coupling strength is represented by the hopping terms, which have different values depending on the type of interaction between neighbors. This extended SSH model is described by an

analytical tight-binding model, whose Hamiltonian has the form

$$H = H_0 + H_{\text{NNN}} \quad (1)$$

where H_0 represents the coupling Hamiltonian between the NNs and intracellular NNNs, and H_{NNN} is the coupling Hamiltonian between the NNNs and the intercellular NNNs. Importantly, the intercellular coupling (highlighted with the red line in Fig. 1) is considered asymmetric, where the hopping occurs only on one of the diagonals describing the first Brillouin zone. In real systems, this results in a slightly asymmetric geometry of the meta-atoms describing the topological system sublattice. The matrix of the Hamiltonian H_0 is given by

$$H_0 = \begin{pmatrix} 0 & \gamma + \alpha e^{-ik_x} & \gamma + \alpha e^{ik_y} & \beta e^{-ik_x + ik_y} \\ \gamma + \alpha e^{ik_x} & 0 & \beta e^{ik_x + ik_y} & \gamma + \alpha e^{ik_y} \\ \gamma + \alpha e^{-ik_y} & \beta e^{-ik_x - ik_y} & 0 & \gamma + \alpha e^{-ik_x} \\ \beta e^{ik_x - ik_y} & \gamma + \alpha e^{-ik_y} & \gamma + \alpha e^{ik_x} & 0 \end{pmatrix} \quad (2)$$

where γ and α are the hopping between the inter- and intracellular NNs, respectively, and β is the hopping between the intracellular NNNs. Next, the matrix Hamiltonian H_{NNN} is written as

$$H_{\text{NNN}} = \begin{pmatrix} 0 & 0 & 0 & Q_1 \\ 0 & 0 & Q_2 & 0 \\ 0 & Q_2^* & 0 & 0 \\ Q_1^* & 0 & 0 & 0 \end{pmatrix} \quad (3)$$

with the matrix elements

$$Q_1 = \lambda(e^{ik_x + ik_y} + e^{-ik_x - ik_y}), \\ Q_2 = \rho e^{-ik_x - ik_y} + \lambda(e^{-ik_x + ik_y} + e^{ik_x - ik_y}). \quad (4)$$

Here, λ and ρ represent the hopping between the remaining NNNs, shown in Fig. 1. In the proposed tight-binding model, we set the strongest hopping term α , while the other hopping terms decay progressively, as shown in the table in Fig. 1(b). In order to split the edge states into type-II and -III corner states, the value of ρ is 0.5α . Figure 1(c) displays the band structure obtained from the extended SSH model with the asymmetric intercellular coupling ρ and the hopping term relationship of Fig. 1(b). This coupling ratio allows obtaining the HOTI phase in the model, which is confirmed by analyzing the topology of the bands below the gap. In this case, only one band is below the gap and the topological characteristics are obtained by the topological invariant

$$\theta^{\text{Zak}} = \int_{\text{BZ}} dk_x dk_y \text{Tr}[A_j(k_x, k_y)], \quad (5)$$

where $A_j(k_x, k_y) = i\langle \psi_j | \partial_k | \psi_j \rangle$ is the Berry connection, $|\psi_j\rangle$ represents the periodic parts of the Bloch function, and j represents the band index. Using Eq. (5) for the first band below the gap, we obtained a $\theta^{\text{Zak}} = (\pi, \pi)$, which indicates that this system is in a nontrivial configuration of the HOTI phase [13,45,49]. Subsequently we can calculate the 2D polarization related to the Zak phase by means of the relation $\theta^{\text{Zak}} = 2\pi\mathbf{P}$ and thus predict the existence of the corner states by means of

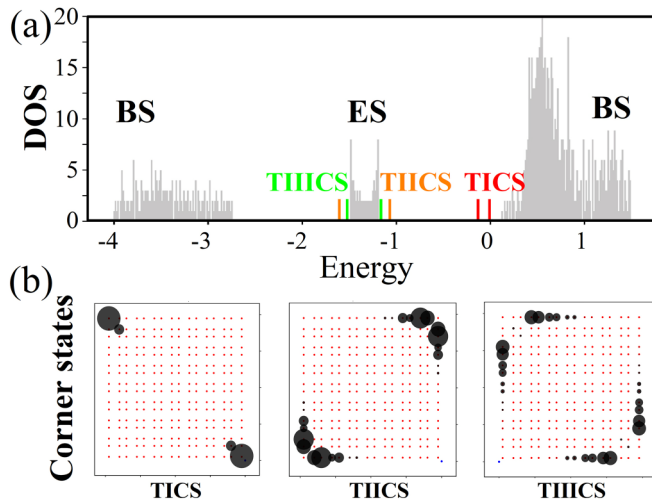


FIG. 2. Characterization of the extended 2D SSH model. (a) Density of states (DOS) of the finite model, where the bulk states (BS), edge states (ES), and different types of corner states are identified. Here the type-I corner states are located near zero energy, while the type-II and -III corner states are found splitting from the edge states continuum. (b) Probability density in a finite model consisting of 8×8 unit cells. The panels from left to right show the corner states type I, type II, and type III, respectively.

the corner charge q^{corner} , defined as [13,45,49]

$$q^{\text{corner}} = 4P_x P_y. \quad (6)$$

Therefore, the corner charge we obtained is 1, indicating the presence of midcorner states of the band gap. The density of states (DOS) for our model with 8×8 unit cells is shown in Fig. 2(a) and reflects the bulk bands and edge bands, in addition to the spectral position of the corner states. Here, we show that the type-I corner states are located at zero energy, while the type-II and -III corner states are located near the energy of the edge states. Due to the asymmetry provided by the hopping term ρ , the type-I states are spectrally separated in pairs: two at zero energy and two very close to zero energy. Notably, as the hopping amplitude $\rho < \alpha, \beta, \gamma, \lambda$, only the type-I corner states arise. Meanwhile, as the strength of ρ gets larger, the type-II corner states emerge and are located near the edge bands within the band gap. In contrast, as the hopping term ρ becomes sufficiently large, type-III corner states arise by splitting from the continuum of edge states found within the band gap.

The probability densities for the three types of corner states in the extended SSH model are shown in Fig. 2(b). Here, the probability density of the type-I corner states is strongly localized at the first site of the topological corner of the lattice. Meanwhile, the type-II corner states exhibit a probability density mostly located in the second unit cells around the topological corner of the square lattice, which agrees with the results presented in other works [35,48]. In contrast, as the hopping term ρ becomes sufficiently large, type-III corner states arise around the topological corner, mainly in the third unit cells, as shown by the probability density in the last panel of Fig. 2(b).

To gain a deeper insight into the origin of the type-III corner states, we add an additional term to the matrix element Q_1 , equivalent to $\rho_1 e^{ik_x - ik_y}$. With this new term, the extended SSH model is represented by the inset in the upper panel of Fig. 3(a). In this case, the coupling between the NNN is symmetric. By adding the new hopping term ρ_1 and making it equal to ρ , the type-III corner states no longer exist, as shown by the DOS in Fig. 3(a). Only type-II corner states arise in the system only if the values of ρ_1 and ρ are equal and large enough to split the corner states from the edge states. As ρ and ρ_1 become smaller, only type-I corner states are present, as shown in the lower panel of Fig. 3(a). Subsequently, we generalize these results in Figs. 3(c) and 3(d), showing the spectrum of eigenenergies as a function of the ratio ρ/ρ_1 , and for the case where $\rho = \rho_1$, respectively. Thus, we observe how type-III corner states arise as they split from the continuum of edge states only when the difference between ρ and ρ_1 is very large, i.e., when the coupling provided by ρ is much stronger than that of ρ_1 . On the other hand, if the equality between ρ and ρ_1 is preserved, type-III corner states do not emerge in this extended SSH model with a square lattice; only type-II states are effectively separated from the edge states. Here, the symmetry breaking in the coupling strength provided by the hopping terms ρ and ρ_1 extracts the type-II corner state branches from the edge state boundaries and the type-III corner state branches from the continuum of edge states. This result shows not only that the addition of coupling between NNNs is necessary to generate type-III corner states, but also an asymmetry in the hopping terms can help generate type-III corner states. Additionally, these results are supported by works that have recently found that 2D square lattices with low symmetry could form HOTIs with corner states, as long as the values of intercellular hopping terms (γ) between NNs are sufficiently small [50,51].

III. EXTENDED PHOTONIC SSH MODEL

PhCs, considered as arrays of artificial atoms, are widely used to modulate electromagnetic waves. In addition, they have recently been used to study topological effects as they have a photonic band structure. Therefore, we have implemented our photonic model in a square lattice PhC slab with a dielectric permittivity $\varepsilon = 12.32$, readily available for experimental fabrication. The tight-binding model we propose in this paper has an asymmetric coupling that causes the splitting of the edge states to generate the type-II and type-III corner states. For this reason, it is imperative to generate this feature in our photonic system.

Let us consider a regular square lattice of circular air holes in a dielectric material, as shown in Fig. 4(a). The unit cell of this system would be described by the four sites shown in the second panel of Fig. 4(a). Here, due to the separation of the holes, coupling between intercellular NNNs is not considered, unlike the strong couplings between intracellular NNNs, which are taken into account. This symmetric picture can be modeled with the extended SSH Hamiltonian without the intercellular NNN couplings. Afterward, to induce the coupling that mimics the hopping term ρ , we extend a semimajor axis, transforming the circular geometry of the air hole to an elliptical one [see third and fourth panels of Fig. 4(a)]. Therefore,

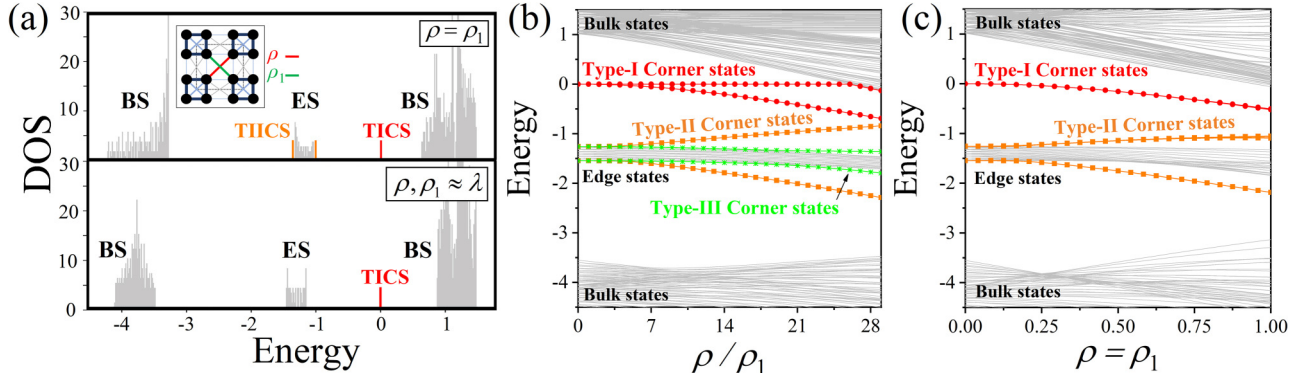


FIG. 3. (a) Upper panel: DOS of the extended 2D SSH model with the hopping terms $\rho = \rho_1$. In this model, only the type-II corner states split from the corner states, while the type-I corner states remain near zero energy. Lower panel: DOS of the extended 2D SSH model preserving the equality between ρ and ρ_1 ; however, they now have a value that approximates to λ . (b) The spectrum of eigenenergies as a function of the ratio ρ/ρ_1 , where $\rho_1 = 1$. The red (circle), orange (square), green (asterisk), and gray curves represent the states of type-I corner, type-II corner, type-III corner, and bulk-edge states, respectively. (c) Eigenenergy spectrum as a function of the equality $\rho = \rho_1$. Here, only the type-I corner and type-II corner states are predicted.

by increasing the semimajor axis of the elliptical air hole, we would be increasing the coupling related to the hopping term ρ .

A regular PhC with the UC1 shown in the first panel of Fig. 4(b) describes a trivial topology. By choosing a UC2, as the one shown in the first lower panel of Fig. 4(b), a PhC with nontrivial topology is obtained. This is demonstrated by analyzing the topological properties of the band structure obtained for both UCs. Both UCs show an identical

photonic band structure, which is shown in the central panel of Fig. 4(b). Here, the band structure has frequency units normalized to the lattice parameter (a) and λ is a wavelength. For this band-structure calculation, we consider only the TE modes (i.e., the modes with electric components parallel to the PhC plane). We performed numerical simulations of the band structure by the COMSOL MULTIPHYSICS software, using the finite element method (FEM), and we solve the eigenvalue problem for the harmonic mode with frequency ω derived from Maxwell's equations [22]:

$$[\nabla^2 + (\omega^2/c^2)\epsilon(\mathbf{r})]\mathbf{E} = 0 \quad (7)$$

where \mathbf{E} is the electric field, $\epsilon(\mathbf{r})$ is the position-dependent permittivity, and c is the speed of light. The Faraday relation gives the magnetic field $\mathbf{H} = -[i/\mu_0\omega]\nabla \times \mathbf{E}$, where the permeability μ_0 is that of the vacuum. Next, we impose periodic boundary conditions at the edges of both unit cells. The lattice parameters describing the PhC of both UCs have lattice parameter a , while the ellipse has a semimajor axis r_a and a semiminor axis $r_b = 0.65r_a$, and is inclined at 45° . For the three-dimensional model, the thickness of the PhC slab is $0.53a$; however, the model can be reduced to a two-dimensional one by considering an effective dielectric permittivity of $\epsilon_{\text{eff}} = 11.5$.

Having computed the band structure of the PhC, we obtained the topological invariant of interest. In this case, we are again interested in the 2D Zak phase or 2D polarization \mathbf{P} . Applying group theory to Eq. (5), one finds that the values of \mathbf{P} are quantized and can only take values of 0 and $1/2$, determined by the parity of the bulk states at the points of high symmetry in the first Brillouin zone [45,52]. Hence, Eq. (6) takes the form

$$P_m = \frac{1}{2} \left(\sum_j q_m^j \bmod 2 \right), \quad (-1)^{q_m^j} = \frac{\eta(\chi_m)}{\eta(\Gamma)}, \quad (8)$$

where the summation is taken over all occupied bands, η denotes the parity with π rotation, and m stands for x or y . Since there is only one band below the gap, Eq. (7) is reduced

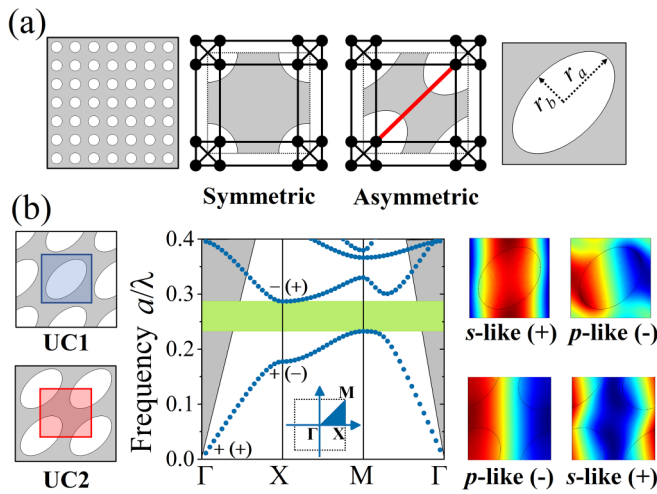


FIG. 4. Photonic model mimicking the extended 2D SSH model with asymmetric coupling. (a) Representation of the PhC design process featuring an asymmetric coupling by extending the semimajor axis of an elliptical geometry of an air hole. The semimajor axis is represented by r_a , while the semiminor axis is r_b . (b) Selection of the unit cells (UC1 and UC2) used for the topological PhC design. The central panel shows the photonic band structure corresponding to UC1 and UC2, where the parities at the high-symmetry points Γ and X are indicated. These parities are determined from the H_z field distribution shown to the right of the band structure. The top two modes correspond to UC1 at the X points for the first and second bands. The bottom two modes correspond to the UC2.

to

$$P_m = \frac{1}{2}(q_1 \bmod 2), \quad (-1)^{q_1} = \frac{\eta_1(X)}{\eta_1(\Gamma)}. \quad (9)$$

Here, one can determine the η_1 parity by the distribution of the H_z field of the eigenstate at the high-symmetry points. The H_z field distributions corresponding to the eigenstates at the X points are depicted in Fig. 4(b). For UC1, the eigenstate at the X point of the first band has an s -like mode, while the second band at the X point is a p -like mode. In contrast, in UC2 this behavior is the opposite, indicating a band inversion. Subsequently, we determined the parity of the eigenmode profile by the inversion operation relative to the center of the UC. Therefore, s -like modes have a “+” parity, while p -like modes have a “-” parity. The parities of the high-symmetry points X and Γ are presented in the band structure of Fig. 3(c), noting the parity inversion at X points between the two bands. By substituting these results into Eq. (8), a polarization with $\mathbf{P} = (0, 0)$ is obtained for UC1, indicating a trivial topology. Meanwhile, a polarization $\mathbf{P} = (1/2, 1/2)$ is determined for UC2, indicating nontrivial topology. Again, Eq. (6) dictates that the corner charge $q^{\text{corner}} = 1$ for the photonic model, indicating the presence of corner states within the photonic gap.

IV. CORNER STATES IN THE EXTENDED PHOTONIC SSH MODEL

To investigate the corner states arising in the photonic model, we design a boxlike configuration. In this sense, the nontrivial structure with $\mathbf{P} = (1/2, 1/2)$ is surrounded by the trivial structure with $\mathbf{P} = (0, 0)$. Subsequently, Fig. 5(a) shows the topological photonic model obtained using the trivial UC1 and nontrivial UC2. To numerically simulate this photonic model, we apply the FEM method, using perfectly matching layers and scattering boundary conditions to simulate a finite model. The spectrum of the eigenfrequencies obtained from the proposed photonic model is shown in Fig. 5(b), where we have located the corner states. Here, the spectral position of the three types of corner states coincides remarkably well with the previously proposed tight-binding model.

The distribution of TE modes in the PhC shown in Figs. 6(a)–6(c) corresponds to the type-I, type-II, and type-III corner states, highlighted in the eigenfrequency spectrum in Fig. 5(b). Clearly, we see how the field distribution matches with the probability density distribution calculated in the analytical model, particularly for the case where $\rho > \rho_1$. In the type-I corner state [Fig. 6(a)], the field distribution is mostly located in the unit cell describing the topological corner of the nontrivial structure. Then, the type-II corner state is mostly located in the second unit cells of the nontrivial corner [Fig. 6(b)]. Finally, the type-III corner state is strongly localized in the third unit cell that delimits the nontrivial corner [Fig. 6(c)]. This agrees with other results presented in the literature, where it is specified that the type-II and -III corner states, found in systems other than photonic, show a localization surrounding the nontrivial corner. Furthermore, the occurrence of the corner states around the topological corner supports the notion that these corner states are formed

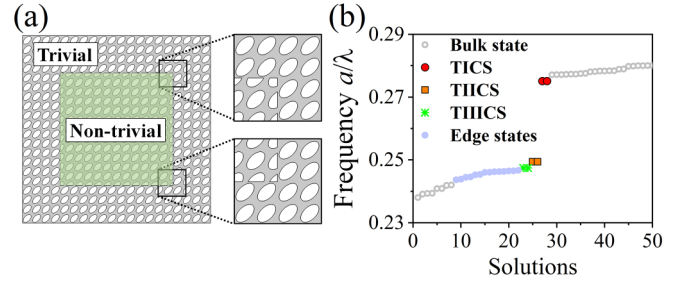


FIG. 5. (a) Box-shaped arrangement of a topological PhC. The nontrivial structure is represented by the inner PhC, while the trivial one describes the outer PhC. (b) Photonic spectrum of eigenfrequencies found in the photonic PhC array, where the type-I, -II, and -III corner states are located, as well as the spectral position of bulk and edge states.

from splitting the edge states within the band gap. It is worth noting that the field distribution of the different corner states in the photonic model coincides almost perfectly with the probability density obtained from the tight-binding model. This highlights how accurate our proposed extended SSH model can be in predicting the existence of corner states in photonic topological systems.

In the proposed photonic model, if we increase the value of the semiminor axis, the type-III corner states tend to disappear, degenerating with the continuum of the edge states. This is also true for the type-II corner states. However, the existence of the latter no longer depends so heavily on the size of the semiminor axis, but rather on the relationship of the lattice parameter a with the semimajor axis. In this regard, we performed a study of the photonic model in which the structural parameters of the ellipse forming the air holes of the topological PhC were altered to match the case analyzed in Sec. II. In particular, we enforced the relation $r_a = r_b$, to mimic the condition $\rho = \rho_1$ in the tight-binding model previously proposed in this paper. The results of this analysis are shown in the second panel of Fig. 6 where the relation $r_a = r_b$ is reflected in the unit cells of Fig. 6(d). By performing a boxlike configuration similar to that shown in Fig. 5(a), we obtained the eigenfrequency photonic spectra of the structure composed of the unit cells in Fig. 6(d). Here, it can be seen that only the type-I state in the middle of the photonic band gap arises, which is in agreement with the results presented in other works. This analysis further confirms the remarkable agreement of the tight-link model with the photonic model, where the manipulation of the hopping terms results in the emergence of type-II and type-III corner states.

Finally, we analyzed the effect of severe structural defects on the proximity of different corner states. For this purpose, we use a systematic method in which one air hole at a time is removed consecutively on the main diagonal of the nontrivial PhC [53,54]. The defect that is removed is labeled N_d where d is the order of the position with respect to one of the topological corners. Figure 7(a) shows the process of removal of elliptical air holes in one of the main diagonals of the nontrivial PhC comprising the topological photonic system.

The analysis of the robustness of the corner states was performed by means of the behavior of the quality factor Q

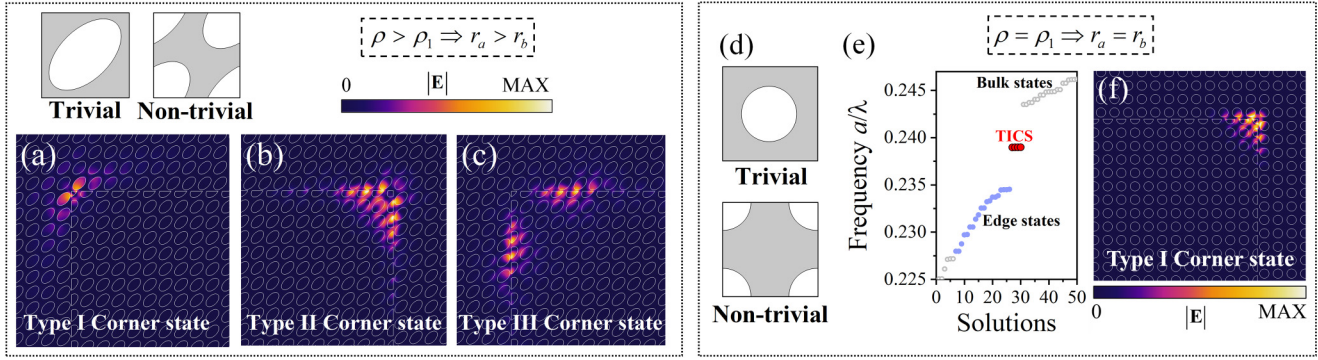


FIG. 6. (a)–(c) E-field distribution corresponding to corner state type I, II, and III, respectively. The corner states found were obtained with geometrical values of the ellipse shown in the upper part. Here, it is shown that the relation $\rho > \rho_1$ translates into $r_a > r_b$ in the photonic regime. (d) Unit cells used for the characterization of a topological PhC where the relation between the hopping terms $\rho = \rho_1$ is realized in the photonic regime with the relation between the structural parameters $r_a = r_b$. (e) Photonic spectrum corresponding to the topological PhC formed with the unit cells of (d). Only the appearance of type-I corner states arises in the middle of the photonic gap and the field distribution is shown in (f).

in the presence of severe structural defects. In this regard, Figs. 7(b)–7(d) show the dependence of the Q_{TICS} , Q_{THCS} , and Q_{THCS} factors on the different N_d defects, where d ranges from 1 to 6. The last value of the Q -factor plots corresponds to the case where no structural defects are present. In addition, for visual purposes, in the inset of Figs. 7(b)–7(d), we show the field distribution corresponding to each corner state for the case where the N_2 defect is present. From the robustness analysis of the corner states, we can appreciate that the defects closest to the topological corner (N_1 , N_2 , and N_3) have the largest effect on the Q factors. However, from defect N_4 onwards, the variation of Q tends to be negligible. If we take

the total variation of Q factors from N_1 to the case without defects, we obtain a variation of no more than 1.1%. These results show that in addition to having high Q factors, the type-II and -III corner states have robustness against defects comparable to that of the type-I corner states.

V. CONCLUSION

In summary, we have investigated the effects of LRI on an extension of the 2D SSH model that exhibits an asymmetric coupling between intercellular NNNs. We have shown that the coupling asymmetry allows the separation of corner states from edge states that fall within the band gap of the HOTI phase. In this sense, we predict the existence of type-III corner states in the asymmetric strong-coupling case between intercellular NNNs, favoring the unfolding of the edge state continuum. Once we return the symmetry couplings between intercellular NNNs preserving the strong-coupling regime, the type-III corner states disappear, returning to their original form as edge states. Subsequently, upon leaving the strong-coupling regime between the intercellular NNNs, the type-II corner states also hybridize with the edge states, leaving only the zero-energy type-I corner states isolated in the gap. We confirm the predictions made by the analytical tight-binding model by first-principles calculations on a photonic model made with a topological PhC slab with elliptic air holes tilted at 45° , mimicking the asymmetric coupling of the proposed tight-binding model. In this way, we are able to bring the type-III corner state concept into the photonic regime. These results extend the knowledge we have about how LRIs dictate the behavior of topological states in HOTI phases. Furthermore, we believe that the obtained results allow us to further relate the HOTI concepts to the photonic regime by exploiting the versatility offered by such systems.

ACKNOWLEDGMENTS

The author thanks Centro de Investigación en Materiales Avanzados for providing the resources required to develop

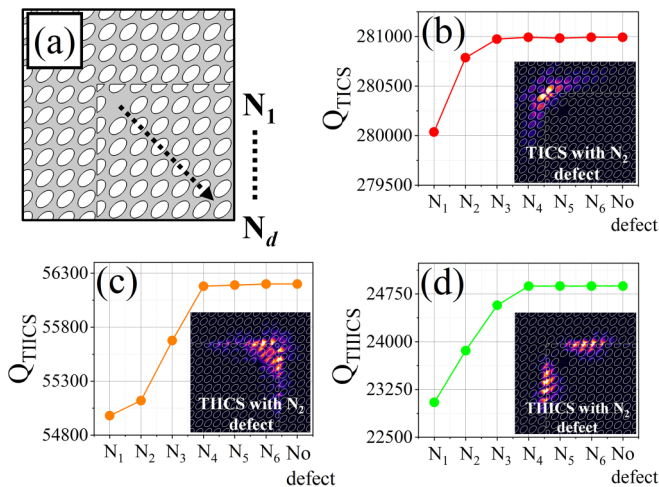


FIG. 7. Analysis of the robustness against disturbances in the three types of corner states. (a) Representation of the hole removal process. The holes are removed systematically and consecutively, starting from the first elliptic hole following the topological corner on the main diagonal of the nontrivial PhC. (b)–(d) Relationship of the Q factors corresponding to each corner state with the different types of defects removed. For visual purposes, the field distribution of each corner state is included to indicate that the field profile does not undergo significant changes.

this research and J. G. Murillo for valuable discussions. The author also wishes to thank the Consejo Nacional de Ciencia y

Tecnología for Grant No. 866231 granted for the development of this research.

- [1] M. Z. Hasan and C. L. Kane, *Rev. Mod. Phys.* **82**, 3045 (2010).
- [2] X.-L. Qi and S.-C. Zhang, *Rev. Mod. Phys.* **83**, 1057 (2011).
- [3] C.-Z. Chang, J. Zhang, X. Feng, J. Shen, Z. Zhang, M. Guo, K. Li, Y. Ou, P. Wei, L.-L. Wang, Z.-Q. Ji, Y. Feng, S. Ji, X. Chen, J. Jia, X. Dai, Z. Fang, S.-C. Zhang, K. He, Y. Wang, L. Lu, X.-C. Ma, and Q.-K. Xue, *Science* **340**, 167 (2013).
- [4] F. D. M. Haldane and S. Raghu, *Phys. Rev. Lett.* **100**, 013904 (2008).
- [5] A. B. Khanikaev and G. Shvets, *Nat. Photonics* **11**, 763 (2017).
- [6] T. Ozawa, H. M. Price, A. Amo, N. Goldman, M. Hafezi, L. Lu, M. C. Rechtsman, D. Schuster, J. Simon, O. Zilberberg, and I. Carusotto, *Rev. Mod. Phys.* **91**, 015006 (2019).
- [7] L.-H. Wu and X. Hu, *Phys. Rev. Lett.* **114**, 223901 (2015).
- [8] Y. Deng, H. Ge, Y. Tian, M. Lu, and Y. Jing, *Phys. Rev. B* **96**, 184305 (2017).
- [9] X. Wu, X. Li, R.-Y. Zhang, X. Xiang, J. Tian, Y. Huang, S. Wang, B. Hou, C. T. Chan, and W. Wen, *Phys. Rev. Lett.* **124**, 075501 (2020).
- [10] S.-Y. Yu, C. He, Z. Wang, F.-K. Liu, X.-C. Sun, Z. Li, H.-Z. Lu, M.-H. Lu, X.-P. Liu, and Y.-F. Chen, *Nat. Commun.* **9**, 3072 (2018).
- [11] H. Fan, B. Xia, S. Zheng, and L. Tong, *J. Phys. D: Appl. Phys.* **53**, 395304 (2020).
- [12] W. A. Benalcazar, J. C. Y. Teo, and T. L. Hughes, *Phys. Rev. B* **89**, 224503 (2014).
- [13] W. A. Benalcazar, B. A. Bernevig, and T. L. Hughes, *Science* **357**, 61 (2017).
- [14] W. A. Benalcazar, B. A. Bernevig, and T. L. Hughes, *Phys. Rev. B* **96**, 245115 (2017).
- [15] Z. Song, Z. Fang, and C. Fang, *Phys. Rev. Lett.* **119**, 246402 (2017).
- [16] J. Langbehn, Y. Peng, L. Trifunovic, F. von Oppen, and P. W. Brouwer, *Phys. Rev. Lett.* **119**, 246401 (2017).
- [17] F. Schindler, A. M. Cook, M. G. Vergniory, Z. Wang, S. S. P. Parkin, B. A. Bernevig, and T. Neupert, *Sci. Adv.* **4**, eaat0346 (2018).
- [18] O. Zilberberg, S. Huang, J. Guglielmon, M. Wang, K. P. Chen, Y. E. Kraus, and M. C. Rechtsman, *Nature (London)* **553**, 59 (2018).
- [19] B. J. Wieder and B. A. Bernevig, *arXiv:1810.02373*.
- [20] G. van Miert and C. Ortix, *Phys. Rev. B* **98**, 081110(R) (2018).
- [21] M. Ezawa, *Phys. Rev. B* **98**, 045125 (2018).
- [22] W. A. Benalcazar, T. Li, and T. L. Hughes, *Phys. Rev. B* **99**, 245151 (2019).
- [23] E. Lee, R. Kim, J. Ahn, and B.-J. Yang, *npj Quantum Mater.* **5**, 1 (2020).
- [24] X.-L. Sheng, C. Chen, H. Liu, Z. Chen, Z.-M. Yu, Y. X. Zhao, and S. A. Yang, *Phys. Rev. Lett.* **123**, 256402 (2019).
- [25] F. Schindler, M. Brzezińska, W. A. Benalcazar, M. Iraola, A. Bouhon, S. S. Tsirkin, M. G. Vergniory, and T. Neupert, *Phys. Rev. Res.* **1**, 033074 (2019).
- [26] I. Petrides and O. Zilberberg, *Phys. Rev. Res.* **2**, 022049(R) (2020).
- [27] B. Xie, H.-X. Wang, X. Zhang, P. Zhan, J.-H. Jiang, M. Lu, and Y. Chen, *Nat. Rev. Phys.* **3**, 520 (2021).
- [28] B. Bahari, A. Ndao, F. Vallini, A. E. Amili, Y. Fainman, and B. Kanté, *Science* **358**, 636 (2017).
- [29] W. Zhang, X. Xie, H. Hao, J. Dang, S. Xiao, S. Shi, H. Ni, Z. Niu, C. Wang, K. Jin, X. Zhang, and X. Xu, *Light Sci. Appl.* **9**, 109 (2020).
- [30] C. Han, M. Kang, and H. Jeon, *ACS Photonics* **7**, 2027 (2020).
- [31] H.-R. Kim, M.-S. Hwang, D. Smirnova, K.-Y. Jeong, Y. Kivshar, and H.-G. Park, *Nat. Commun.* **11**, 5758 (2020).
- [32] A. Cerjan, M. Jürgensen, W. A. Benalcazar, S. Mukherjee, and M. C. Rechtsman, *Phys. Rev. Lett.* **125**, 213901 (2020).
- [33] W. A. Benalcazar and A. Cerjan, *Phys. Rev. B* **101**, 161116(R) (2020).
- [34] Z.-G. Chen, C. Xu, R. Al Jahdali, J. Mei, and Y. Wu, *Phys. Rev. B* **100**, 075120 (2019).
- [35] M. Li, D. Zhirihin, M. Gorlach, X. Ni, D. Filonov, A. Slobozhanyuk, A. Alù, and A. B. Khanikaev, *Nat. Photonics* **14**, 89 (2020).
- [36] Y. Chen, F. Meng, Z. Lan, B. Jia, and X. Huang, *Phys. Rev. Appl.* **15**, 034053 (2021).
- [37] C. N. Varney, K. Sun, M. Rigol, and V. Galitski, *Phys. Rev. B* **82**, 115125 (2010).
- [38] W. Beugeling, J. C. Everts, and C. Morais Smith, *Phys. Rev. B* **86**, 195129 (2012).
- [39] S. Shen, C. Li, and J.-F. Wu, *Opt. Express* **29**, 24045 (2021).
- [40] N. A. Olekhno, A. D. Rozenblit, V. I. Kachin, A. A. Dmitriev, O. I. Burmistrov, P. S. Seregin, D. V. Zhirihin, and M. A. Gorlach, *Phys. Rev. B* **105**, L081107 (2022).
- [41] X.-L. Yu, L. Huang, and J. Wu, *Phys. Rev. B* **95**, 125113 (2017).
- [42] D. Leykam, S. Mittal, M. Hafezi, and Y. D. Chong, *Phys. Rev. Lett.* **121**, 023901 (2018).
- [43] X.-D. Chen, W.-M. Deng, F.-L. Shi, F.-L. Zhao, M. Chen, and J.-W. Dong, *Phys. Rev. Lett.* **122**, 233902 (2019).
- [44] B.-Y. Xie, G.-X. Su, H.-F. Wang, H. Su, X.-P. Shen, P. Zhan, M.-H. Lu, Z.-L. Wang, and Y.-F. Chen, *Phys. Rev. Lett.* **122**, 233903 (2019).
- [45] Y. Ota, F. Liu, R. Katsumi, K. Watanabe, K. Wakabayashi, Y. Arakawa, and S. Iwamoto, *Optica* **6**, 786 (2019).
- [46] X. Zhang, H.-X. Wang, Z.-K. Lin, Y. Tian, B. Xie, M.-H. Lu, Y.-F. Chen, and J.-H. Jiang, *Nat. Phys.* **15**, 582 (2019).
- [47] C. Poli, H. Schomerus, M. Bellec, U. Kuhl, and F. Mortessagne, *2D Mater.* **4**, 025008 (2017).
- [48] H. Yang, L. Song, Y. Cao, and P. Yan, *Phys. Rev. B* **106**, 075427 (2022).
- [49] B.-Y. Xie, H.-F. Wang, H.-X. Wang, X.-Y. Zhu, J.-H. Jiang, M.-H. Lu, and Y.-F. Chen, *Phys. Rev. B* **98**, 205147 (2018).
- [50] K.-H. Kim, *Ann. Phys. (NY)* **533**, 2100075 (2021).
- [51] K.-K. Om and K.-H. Kim, *Phys. Status Solidi B* **258**, 2100202 (2021).
- [52] C. Fang, M. J. Gilbert, and B. A. Bernevig, *Phys. Rev. B* **86**, 115112 (2012).
- [53] X. Xie, J. Dang, S. Yan, W. Zhang, H. Hao, S. Xiao, S. Shi, Z. Zuo, H. Ni, Z. Niu, X. Zhang, C. Wang, and X. Xu, *Opt. Express* **29**, 30735 (2021).
- [54] J. A. Medina-Vázquez, J. G. Murillo-Ramírez, E. Y. González-Ramírez, and S. F. Olive-Méndez, *J. Appl. Phys.* **132**, 133104 (2022).